International Journal of Impact Engineering 156 (2021) 103940

Contents lists available at ScienceDirect

International Journal of Impact Engineering

journal homepage: www.elsevier.com/locate/ijimpeng

The Taylor–Quinney coefficients and strain hardening of commercially pure titanium, iron, copper, and tin in high rate compression

G.C. Soares *, M. Hokka

Impact – Multiscale Mechanics Research Group, Engineering Materials Science, Materials Science and Environmental Engineering, Faculty of Engineering and Natural Sciences, Tampere University (TAU), Tampere, Finland

ARTICLE INFO

Keywords:
Adiabatic heating
Taylor–Quinney coefficient
Infrared thermography
High strain rate
Thermomechanical behavior
Strain hardening

ABSTRACT

This work presents an investigation on the effects of adiabatic heating and strain rate on the dynamic compressive response of titanium, iron, copper, and tin. The high strain rate tests were carried out with a Split Hopkinson Pressure Bar (SHPB) and the low strain rate tests with a servohydraulic testing machine. The temperature increase of the specimens during deformation was measured with high speed infrared thermography (IRT). The results show that all the investigated materials have positive strain rate sensitivity and temperature increases of up to 65 °C were observed in the high strain rate experiments (500–3100 s^{-1}). Adiabatic heating in all investigated materials increased with strain rate. The temperature increase at the strain rate of 1 s^{-1} clearly diminished the strain hardening rate of iron and titanium but was seemingly insufficient to impact the mechanical behavior of copper and tin. The Taylor–Quinney coefficients (β_{int} and β_{diff}) were found to be strain and strain rate dependent. At higher strain rates (1200–3100 s^{-1}), the integral β_{int} was smaller in the beginning of the test (0.2 to 0.7) and increased to approximately 0.8–0.9 at larger plastic strains. The differential β_{diff} comprised gaussian curves as a function of strain whose maximum values were from 0.9 to 1.2 for the investigated materials. Tin had lower β_{int} and β_{diff} with higher strain hardening rates, while copper had a higher β_{int} and β_{diff} with a low strain hardening rate throughout the high strain rate tests. These results indicate that copper had a more stable microstructure during deformation and converted most of the applied plastic work into heat, while tin had a faster evolving microstructure which stored more plastic work in its microstructure during plastic deformation. Furthermore, this suggests that β_{int} and β_{diff} can be used as parameters to investigate the stability and the microstructural evolution of materials under high strain rate plastic deformation. β_{diff} is more appropriate to describe the instantaneous thermomechanical behavior of a material and β_{int} is more appropriate for applications which benefit from a single parameter to characterize how efficiently a material converts plastic work into heat up to a given strain level.

1. Introduction

Materials release considerable amount of heat when deformed rapidly, and this phenomenon occurs on several industrial applications such as forging, rolling and extrusion. This leads to adiabatic heating at high rates of deformation as the heat does not have enough time to dissipate into the surroundings. An increase in the temperature usually decreases the mechanical strength and increases the ductility [1], and can lead to strain localizations, dynamic recrystallization [2], unexpected failure, and development of rough surface quality. Considering its impact in the mechanical behavior of materials, it is fundamental to understand the relationship between adiabatic heating and test parameters such as amount of deformation, strain rate, loading mode as well as material aspects such as crystallographic structure, stacking fault energy, microstructural features and thermomechanical history.

The mechanical behavior of tin [3,4], copper [5,6], iron [7–9], and titanium [10,11] under a multitude of strain rates and temperatures has been already extensively investigated in the published literature. These materials have different crystallographic structures and thus their deformation mechanisms and temperature/strain rate dependencies are different. A pure face-centered-cubic (FCC) metal such as copper normally has a strain rate independent yield strength and a strain rate dependent strain hardening behavior, while a body-centered-cubic (BCC) metal, such as iron, and a hexagonal-close-packed (HCP) metal,

* Corresponding author.
E-mail addresses: guilherme.correasoares@tuni.fi (G.C. Soares), mikko.hokka@tuni.fi (M. Hokka).

https://doi.org/10.1016/j.ijimpeng.2021.103940
Received 3 November 2020; Received in revised form 1 April 2021; Accepted 7 June 2021
Available online 11 June 2021

such as pure titanium, have a very strain rate dependent yield strength and an almost strain rate independent strain hardening behavior [12]. The strong strain rate dependence of the strain hardening in FCC is related to the jog formation and dislocation intersection during deformation amount of which depend strongly on the dislocation density or the amount of plastic strain. The weaker strain rate dependence of strain hardening in the BCC and HCP, on the other hand, is caused by their high lattice friction [12] which does not depend on the amount of deformation. Although dislocation slip is usually the most common deformation mechanism for most metallic alloys at common test temperatures, an increase in strain rate can lead to an increase in mechanical twinning in less symmetrical crystal structures such as tetragonal, orthorhombic, and monoclinic metals [12]. Tin has a body-centered tetragonal (BCT) crystal structure and a complex plastic behavior due to the lower crystallographic symmetry and having many more slip systems than other metals [13]. At high temperatures, dislocation climb may be promoted even during high rate deformation in tin alloys, due to the complexity of the slip characteristics [1]. Nevertheless, despite the fact that the mechanical behavior of these materials has already been studied quite much, the quantitative relationship between adiabatic heating and mechanical behavior and high rate response of the materials are not understood properly. The heat output of the material during adiabatic deformation depends on various material properties including density and heat capacity, but also more importantly the material's capacity to store energy into its microstructure. The last one especially depends on the microscopic mechanisms of plastic deformation and the microstructure evolution of the material. Therefore, understanding the both the current state of the material and its evolution during deformation are important for accurate material modeling as they describe both the material response and how the response evolves during deformation.

The increase in temperature due to adiabatic heating in high strain rate tests occurs very fast, and it is technically challenging to record the temperature, load and strain data accurately and synchronously during these tests. The most commonly used techniques in high speed thermomechanical investigations have been thermocouples, InSb infrared detectors and infrared imaging. Despite their longer response time, Rittel [14–16] has successfully used small thermocouples to investigate the temperature evolution of a specimen during high strain rate loading. InSb infrared detectors have both a short response time [17] and fast acquisition rates [18], which have lead to these sensors having been used in research of dynamic events such as adiabatic shear band formation [19], shear band propagation [17], crack propagation [18], and the release of heat under high strain rate compression [20]. High speed infrared imaging has allowed full-field investigations of dynamic events such as adiabatic heating of titanium and stainless steel in tension at strain rates up to 7000 s^{-1} [21–23], heat generated in ballistic impacts on triaxially braided composites [24], and the formation of adiabatic shear bands in aluminum alloys [25]. The recent advances in high speed temperature measurement techniques have allowed for more intricate investigations of the adiabatic heating in high strain rate deformation of materials and the research of the effects of adiabatic heating on established material parameter such as strain hardening rate and thermal softening.

The work of Taylor, Quinney and Farren [26,27] are the foundation for the systematic study of the thermomechanical coupling effect. In their work, they postulated the Taylor–Quinney coefficient (β), or the Inelastic Heat Function [21], as the ratio between the applied mechanical work and the thermal energy released to the surroundings. The Taylor–Quinney coefficient can be described both in the form of total converted energy converted (β_{int}) and rate of energy conversion (β_{diff}) as shown in Eq (1) and Eq (2). In these equations, C_p, and ρ are the material's heat capacity and density, while T and dW_p are the temperature and incremental plastic work. $\dot{T}$ and $\dot{W}_p$ represent the time derivatives of temperature and incremental plastic work.

$$\beta_{int} = \frac{\rho C_p \Delta T}{\int dW_p} \tag{1}$$

$$\beta_{diff} = \frac{\rho C_p \dot{T}}{\dot{W}_p} \tag{2}$$

By describing the fraction of plastic work converted into heat during plastic deformation, β indirectly also defines how much energy is being stored in the material's microstructure. The evolution of these parameters during plastic deformation could reveal more information on the underlying deformation mechanisms and fundamentals of the microstructure evolution, as these mechanisms can have distinct levels of efficiency in which they convert plastic work into heat [28]. The scientific community has shown interest in understanding the effects of strain, strain rate and loading mode on β in different materials [16,21,29–31]. Rittel et al. [5] investigated the average β_{int} of a single crystal and polycrystalline copper. In their study, the polycrystalline copper had a β_{int} from 0.4 up to 0.65 at high strain rates, while the single crystal had a β_{int} that ranged from 0.6 up to 0.9. Smith et al. [21] investigated the β_{int} of a Ti-6Al-4 V alloy at strain rates of 1 s^{-1} up to 7000 s^{-1} in tension, and reported similar values that increase from approximately 0.4 at lower strains (ε <0.05) up to 0.6 at higher strains (ε >0.15). Rittel et al. [31] investigated the β_{int} on titanium, aluminum alloys, and steels in dynamic compression at strain rates from 2000 s^{-1} to 3000 s^{-1}. The authors reported a β_{int} that decreased from 0.5 to 0.4 with an increase in strain for a Ti-6Al-4 V alloy, and a β_{int} that decreased from 0.9 to 0.7 in commercially pure titanium. According to the authors, the β_{int} of Al 5086 decreased from 0.4 to 0.2 with increase in strain, while the β_{int} of Al 2024 had a constant of approximately 0.3. In their investigation, the 1020 steel had a constant β_{int} of approximately 0.85. Régal and Pierron [30] measured the strain with the grid method and temperature increase with infrared imaging of tin during plastic deformations by Image-Based Ultrasonic Shaking and reported a β of approximately 0.9 for low strain values, which decreased to approximately 0.6 with the increase in strain. Zhang et al. [29] investigated the β_{int} in near α and near β titanium alloys and concluded that the near α alloy had a β_{int} of approximately 0.6 (close to the commercially pure titanium) and the near β alloy had a significantly lower beta of approximately 0.35. Despite the previous efforts, there is no consensus on the reasons for the behavior of β_{int} and more systematic work is required to build enough understanding and a large enough database to evaluate the effects of different variables on β_{int} and β_{diff}. Furthermore, there is also a significant gap in knowledge on what are the quantitative effects of adiabatic heating on the material behavior and what is the exact relationships between the β and the strain hardening behavior as well as how they relate to microstructural evolution.

The novelty of this work lies in combining the dynamic compressive response with high speed temperature measurements to investigate the influence of adiabatic heating and strain rate on the mechanical behavior of four pure metals (Ti, Fe, Cu and Sn) with different crystallographic structures. The Taylor–Quinney coefficients were measured and used to investigate the thermomechanical coupling effect by comparing the strain hardening behavior and the obtained Taylor–Quinney coefficients. The results of this investigation can assist in the development of more accurate material modelling and contributes to the formation of a thermomechanical database of materials.

2. Experimental methods

The investigated materials were commercially pure tin, copper, iron, and titanium. These metals were chosen due to their different crystal structures to investigate the possible influence of this property on adiabatic heating and the thermomechanical coupling effect. The materials were received in rods which were machined into compression specimens by turning on a lathe. The sample dimensions, condition, purity, and crystallographic structure for each material are given in

Table 1
Material crystallographic structure, condition, purity, and dimensions of cylindrical specimens used in this investigation.

Material	Crystal Structure	Condition	Purity (%)	Diameter (mm)	Thickness (mm)
Sn	Body-Centered Tetragonal (BCT)	Extruded	99.75	18.0	7.9
Cu	Face-Centered Cubic (FCC)	Cold-drawn	99.994 (OFHC)	16.0	7.9
Fe	Body-Centered Cubic (BCC)	As drawn	99.95	12.8	8.0
Ti	Hexagonal Close-Packed (HCP)	Annealed	99.6+ (Grade 2)	10.1	8.0

Table 1. The dimensions of the samples were designed so the same setup could be used to reach similar strain rates and total strain for all investigated materials. Compression tests were conducted at a wide range of strain rates from 1.25×10^{-4} up to 3100 s^{-1} and each test was repeated three times. Some experiments failed and only successful experiments are reported in the following. The low strain rate (1.25×10^{-4}–1 s^{-1}) tests were carried out with an Instron 8800 servo-hydraulic testing machine and the high strain rate (500–3100 s^{-1}) tests were performed with a Split Hopkinson Pressure Bar (SHPB).

The SHPB setup is composed of an incident bar, a transmitted bar, a striker bar, and a trap momentum bar. These bars are made of high strength maraging steel and have a 22 mm diameter. The incident, transmitted, and the momentum trap bars were 1200 mm long, and two striker bars with 200 mm and 300 mm length were used. A pair of strain gages were attached to the incident and transmitted bars at a distance of 600 mm from the interface between the bars. The incident, transmitted, and reflected loading pulses were measured with the strain gages, and the signals were amplified with a Kyowa CDV 700A signal conditioner and then finally recorded with a Yokogawa digital oscilloscope. The dispersion of the pulses was corrected with a numerical method based on the work of Gorham and Wu [32]. The dispersion corrected stress pulses were used to calculate stress, strain rate, and strain in the specimen during the high strain rate tests. Further information and examples of the setup and processing of the data can be found in these references [33–35].

The temperature increase (ΔT) of the samples during the mechanical tests was monitored with a Telops FAST-IR-2 K high speed infrared camera. The distance from the camera to the specimen was approximately 75 cm, and the camera was observing the specimen at an angle of approximately 90 ± 1 °. Such a distance between the camera and the specimen was necessary to both fit most of the specimen in the low resolution of high strain rate tests, but also to protect the camera from possible debris and the specimen flying out from the setup after the test. Fig. 1 shows the experimental setups for the low and high strain rate tests. It is not possible to completely shield the camera from infrared radiation from the surroundings. However, the unwanted reflections were minimized using plexiglass covers which prevented most of the scattered IR radiation from reflecting from the specimen towards the camera. The effect of the scattered infrared radiation could have had some influence the measurements at lower temperatures. An integration time of 5 μs and an imaging rate of 90 kHz was used for the high strain rate tests, while an integration time of 100 μs and imaging rates of 0.1, 10 and 1000 Hz were used for the strain rates of 1.25×10^{-4}, 10^{-2} and 1 s^{-1}, respectively. Considering a 5 μs integration time and a 90 kHz acquisition rate, the temperature measurements during the high strain rate tests were made every 11 μs and there was a 6 μs interval between each picture during which no temperature data was acquired. Although the use of a higher acquisition rate would increase temporal resolution and improve the temperature and β measurements, 90 kHz is currently one of the fastest possible acquisition rates for infrared cameras and already comes with a considerable resolution tradeoff (64×4 pixel). Fig. 2 shows examples of the full-field temperature images at different true strains for a titanium specimen.

The onset of data acquisition of both the oscilloscope and the infrared camera were triggered by the incident pulse to ensure temporal

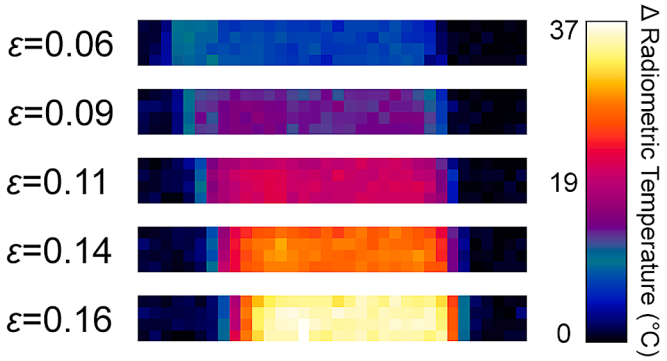

Fig 2. Full-field increase of radiometric temperature images at different true strains for a titanium specimen under compression at a strain rate of 1200 s^{-1}.

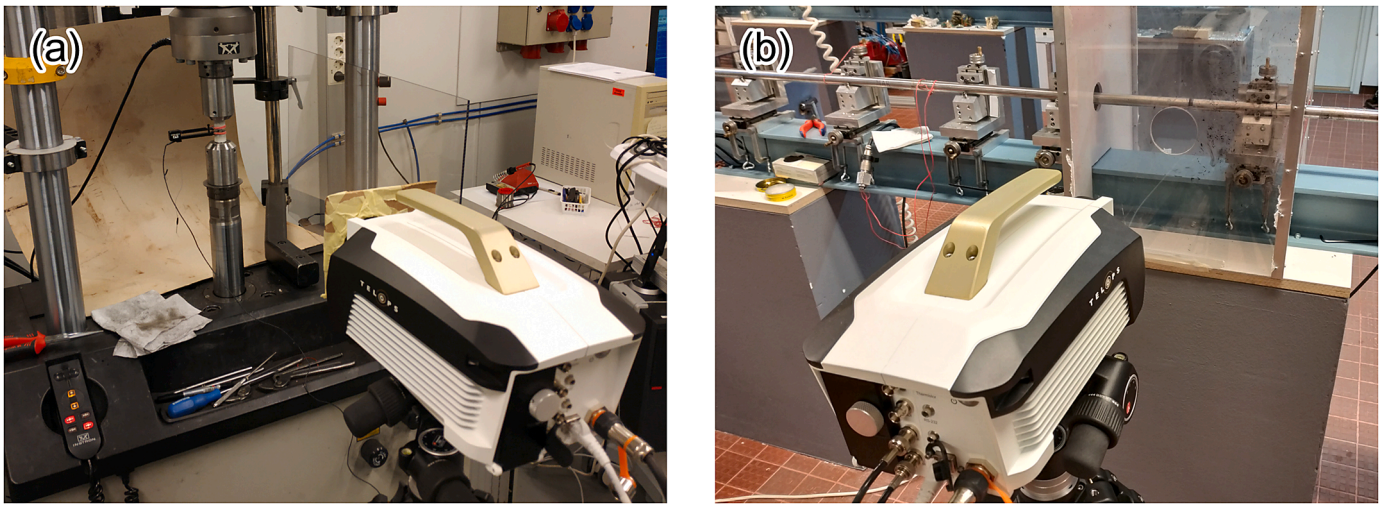

Fig 1. Experimental setup used in the low and high strain rate tests comprised the infrared camera, the servohydraulic testing machine, and the Split Hopinkson Pressure Bar device.

synchronization of the load, strain, and temperature measurements. Fig. 3 shows the strain gage data measured from the stress bars some distance before and after the specimen, the radiometric temperature of the specimen, and trigger out signals from the infrared camera in the same time frame for a high strain rate test on a titanium specimen. The moment at which the stress pulse reaches the specimen and marks the onset of the test is marked with an arrow.

A calibration from radiometric temperature to surface temperature had to be performed, as the infrared camera by default assumes that the target material is a perfect black body with an emissivity of one. The user must convert the measured radiometric temperatures to the true surface temperature of the specimen using either an experimental calibration data or a known constant emissivity to convert the radiometric temperature to true material temperature. A temperature calibration curve was obtained by slowly heating a sample of each metal on a hot plate and simultaneously monitoring their temperature with a type K thermocouple and the infrared camera. For the calibration procedure, the thermocouples were spotwelded to the titanium and iron specimens but given that it was very challenging to spot weld them to copper and tin, a mechanical clamp was used to securely hold the thermocouple against the copper and tin specimens. The heating of the specimen was carried out very slowly so that the temperature of the thermocouple was the same as the surface temperature of the metal specimen. The calibration setup was made so that it would be as close to the compression test setup as possible, in terms of the camera distance, the angle between the camera and the specimens, and acquisition parameters. The calibration procedure was performed up to four times for every investigated material and integration times. In these calibration runs, the average full-field radiometric temperature of the specimen was compared with the surface temperature measured by the thermocouple. The average radiometric temperature was calculated from a 20–40 pixel rectangle in the center of the specimen, in close proximity of the thermocouple. The area was chosen so that the vertical temperature gradients were minimized and the possible reflections from the calibration tools were avoided. A third order polynomial was used to fit this data and to construct the calibration curves. Fig. 4 shows the calibration curves of the investigated materials for an integration time of 5 μs and an example of the temperature distribution during the temperature calibration of a copper specimen. The white dashed rectangle represents an example of the area which was used to calculate the average radiometric temperature during the calibration procedure. Accurate temperature calibration curves are essential for analyzing the thermomechanical behavior of materials, as even a small change in the rate in which temperature increases could have strong influence in the calculation of the Taylor–Quinney coefficient. The uncertainty of the temperature measurements is higher at high acquisition rates and temperatures close to room temperature due to low filling of the sensor and poor signal to noise ratio. Therefore, it is essential to be very careful when calibrating the lower temperature range (20 to 30 °C) in which the relationship between radiometric temperature and surface temperature is not necessarily linear. The images remained focused and the specimen surface stayed within the depth-of-field of the infrared camera throughout the tests, so the different specimen diameters and the expansion of the specimens during compression had only a minor influence on the measurements.

The results are presented as true stress-true plastic strain curves and strain hardening rate, instantaneous strain hardening exponent, instantaneous strength coefficient, and the adiabatic heating, ΔT, as a function of plastic strain. In all figures the solid lines represent the average mean of two or three tests and the dashed lines represent the standard error of the mean. The instantaneous strain hardening exponent and strength coefficient are based on the Hollomon equation (Eq (3)) in which K is the material strength coefficient and n is the strain hardening exponent. A more detailed description of how the instantaneous strain hardening exponent is calculated can be found in references [36–38]. The instantaneous strength coefficient was obtained by solving a point-slope equation using the instantaneous strain hardening exponent as the slope and a point on the logarithm of true stress-true plastic strain, and extrapolating that equation to a true plastic strain of 100%. The Taylor–Quinney coefficients, β_{int} and β_{diff}, were calculated for strain rates from 500 s^{-1} to 3100 s^{-1}. These strain rates were chosen considering that adiabatic conditions are required for the validity of Eq (1) and 2. No temperature gradient between the sample and anvils were observed in the IRT images at these strain rates, which corroborate the assumption that those tests occurred under adiabatic conditions. The tests consisted of a maximum of 15 images and the temperature data was linearly interpolated to match the same amount of data points as that in the stress strain plots. Differentiating a set of only 15 data points would give a noisy signal and therefore the time differentials used for calculations of the β_{diff} were obtained from the interpolated data. The material density and heat capacity used to calculate β_{int} and β_{diff} are shown on Table 2.

$$\sigma = K \cdot \varepsilon^{n} \tag{3}$$

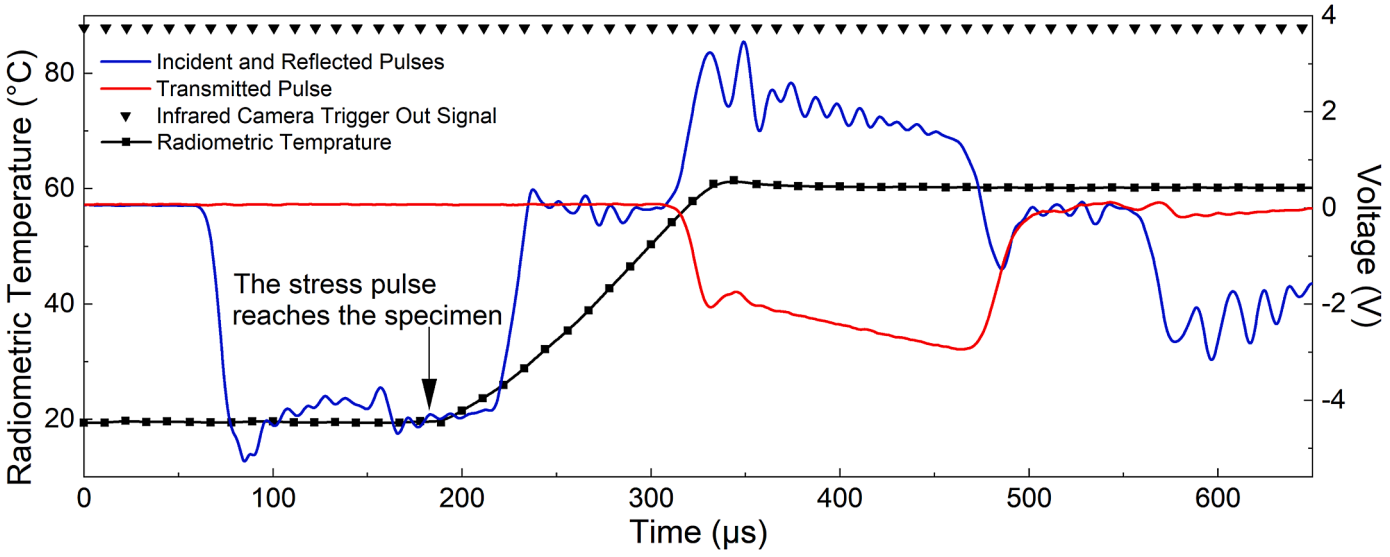

Fig 3. Strain gage signals from the incident and transmitted stress bars, radiometric temperature of the specimen, and trigger out signals from the infrared camera for a titanium specimen tested at a high strain rate. The arrow marks the moment at which the incident stress pulse reaches the specimen.

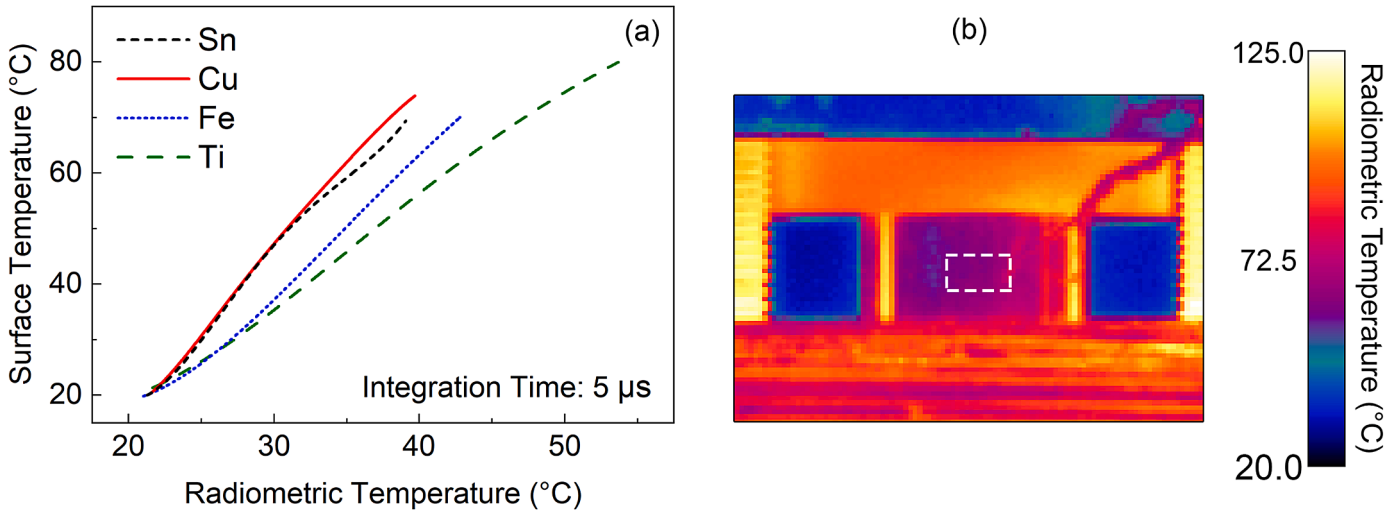

Fig 4. (a) Surface temperature as a function of radiometric surface temperature for Sn, Cu, Fe and Ti with an integration time of 5 μs and (b) example of radiometric temperature distribution of a copper specimen during temperature calibration. The white dashed rectangle represents the area from which the average temperature was calculated.

Table 2
Thermophysical properties of the investigated materials [39].

Material	Density (kg/m^3)	Heat Capacity (J/kg K)
Sn	5765	205
Cu	8930	384.6
Fe	7870	447.3
Ti	4507	522.3

3. Results

The compression tests were performed at strain rates from 1.25×10^{-4} to 3100 s^{-1} with total true strains ranging from 0.05 up to 0.35. The total strain observed in some the tests from 500 to 600 s^{-1} were considerably lower than in the higher strain rate experiments, due to the required lower striker speed necessary to perform these tests. Fig. 5 shows the measured temperature increase ΔT of the specimen as a function of true plastic strain. The temperature increase at strain rates of 1.25×10^{-4} and 10^{-2} s^{-1} was understandably the lowest, as considering the time those tests took, there was substantial heat transfer from the sample to the surroundings. A maximum ΔT of approximately 65 °C was observed for titanium at the strain rate of 2300 s^{-1} and 0.18 plastic strain. Generally, the temperature increase rate at the strain rate of 1 s^{-1} was lower than that at higher strain rates. However, the temperature increase rate of tin and copper at the strain rate of 1 s^{-1} was one order of magnitude lower than that observed at the strain rate of 1000 s^{-1}, which could be related to the evidently lower applied plastic work at the strain rate of 1 s^{-1} which is observed in the stress-strain plots. Although the temperature rise of copper is considerably lower at the strain rate of 1 s^{-1} than that observed at higher strain rates, its flow stress at the strain rate of 1 s^{-1} is only 25% lower than the flow stress at higher rates. Therefore, it is possible that the lower temperature rise is not entirely explained only by the lower applied plastic work.

The true stress-true plastic strain curves are shown in Fig. 6. A positive strain rate sensitivity was observed for all investigated materials. Titanium had the highest flow stress of approximately 1000 MPa at 0.17 plastic strain and at strain rate of 2300 s^{-1}, while tin had the flow stresses as low as 10 MPa at 0.33 plastic strain and at strain rate of 1.25×10^{-4} s^{-1}. Iron showed only modest hardening at the lowest strain rates (1.25×10^{-4} to 10^{-2} s^{-1}), which decreased even further with increasing strain rates. At higher strain rates (500–2400 s^{-1}) even strain softening was observed for iron, probably due to adiabatic heating and reduced dynamic recovery at high strain rates. Copper had a positive strain rate sensitivity with low strain hardening. Tin demonstrated a peculiar stress-strain behavior, and the results for the tests at lower strain rates (1.25×10^{-4} to 1 s^{-1}) and the higher strain rates (1000 and 1700 s^{-1}) are considerably different. At lower strain rates, the stress-strain curves show a single smooth strain hardening behavior, while at higher strain rates, the stress-strain curves clearly show two regions of strain hardening: the first stage with a rapid hardening until approximately 0.07 plastic strain and the second stage with an almost ideal plastic behavior and very little hardening. The effect of adiabatic heating on the strength of the material (flow stress) at the strain rate of 1 s^{-1} is evident for titanium and iron, as the strain hardening rate is clearly lower than that observed at lower strain rates. The stress-strain curve at the strain rate of 10^{-2} s^{-1} would seemingly cross the stress strain curve at strain rate of 1 s^{-1} if higher strains had been imposed.

The strain hardening rate describes the rate at which true stress increases as a function of true strain and can be obtained as the derivative of the stress-strain curves in Fig. 6. The strain hardening rate as a function of plastic strain of the compression tests is shown in Fig. 7. The strain hardening rate of titanium did not change much as a function of strain rate. Compared to the other materials, titanium had the highest strain hardening rates. The strain hardening rate of iron was rather low at low strain rates (1.25×10^{-4} to 10^{-2} s^{-1}), and the hardening rate further decreased with an increasing strain rate and eventually became negative at higher strain rates (1 to 2400 s^{-1}). The decrease in the strain hardening rate due to adiabatic heating with an increase in strain rate from 10^{-2} to 1 s^{-1} was evident for titanium and iron. Copper had a very low strain hardening rate at low strain rates, which slightly increased at higher strain rates. At low strain rates (1.25×10^{-4} to 10^{-2} s^{-1}) the strain hardening rate of tin was very low and it did not change much with increasing strain rate in the quasi-static regime. At higher strain rates (1000–1700 s^{-1}), the strain hardening rate of tin was much higher at small strains and then at larger plastic strains the strain hardening rate was close to zero.

Fig. 8 shows the instantaneous strain hardening exponent as a function of true plastic strain. The instantaneous strain hardening exponent of titanium was similar at most investigated strain rates, it steadily increased from 0 to approximately 0.25 at plastic strains of 0.15. However, instantaneous strain hardening exponent was considerably lower and only reached a valued of 0.15 at the strain rate of 1 s^{-1}, condition in which the temperature increase was higher and had a more prominent role in the mechanical behavior of the material. The instantaneous strain hardening exponent of iron increased from 0 up to 0.15 as

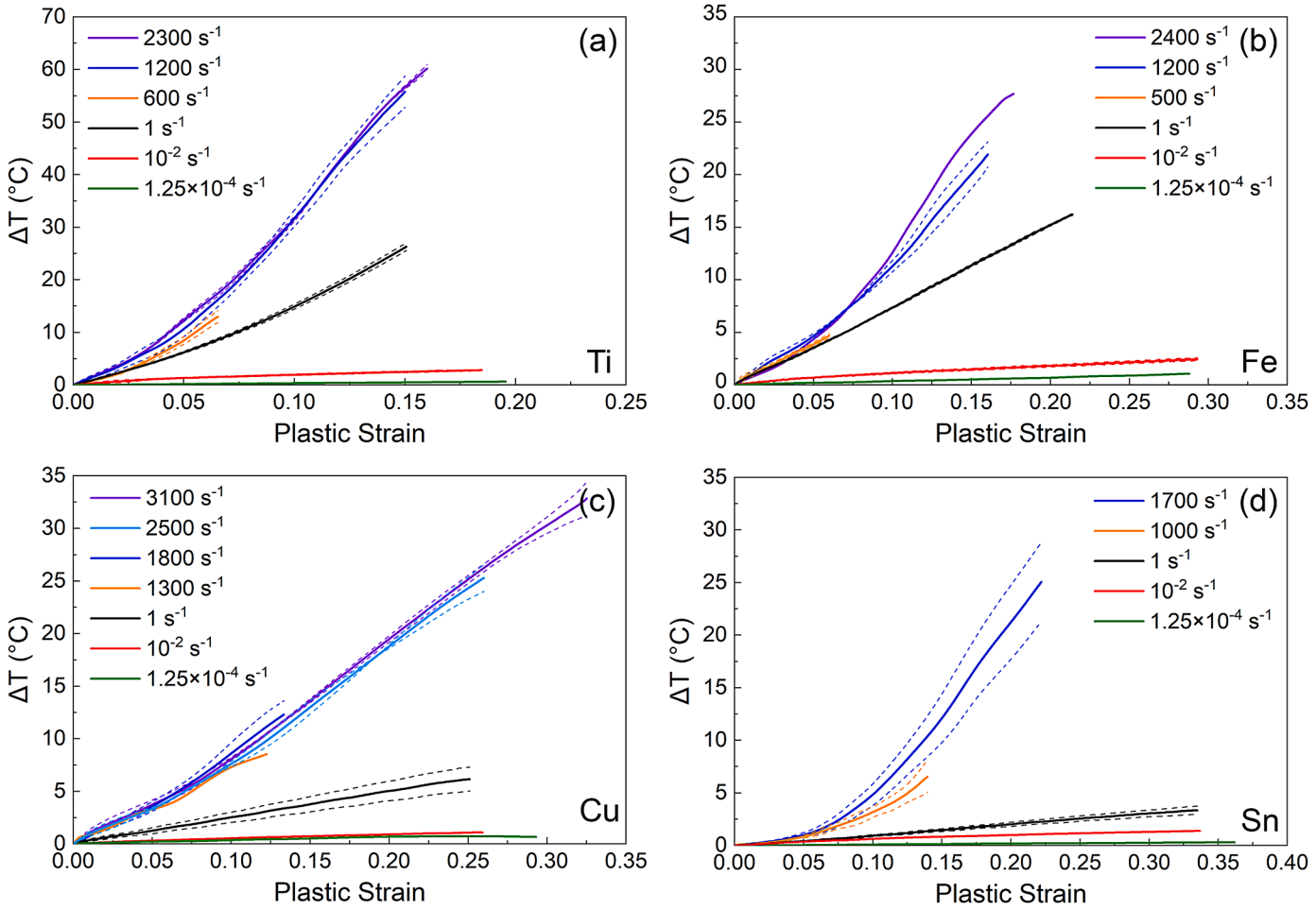

Fig 5. Temperature increase as a function of plastic strain for Ti (a), Fe (b), Cu (c) and Sn (d) at strain rates from 1.25×10^{-4} to 3100 s^{-1}.

a function of strain at strain rates of 1.25×10^{-4} and 10^{-2} s^{-1}, and instantaneous strain hardening exponent was generally lower at the strain rate of 1 s^{-1} due to the influence of adiabatic heating. At higher strain rates (500–2400 s^{-1}) strain softening was observed and the instantaneous strain hardening exponent was not appropriate for analyzing the mechanical behavior of iron in those strain rates. At lower strain rates (1.25×10^{-4} to 1 s^{-1}), the instantaneous strain hardening exponent of copper increased from 0 to approximately 0.15 at plastic strains of 0.25. In general, the instantaneous strain hardening exponent was approximately 0.1 throughout plastic deformation at high strain rates. The instantaneous strain hardening exponent of tin increased with strain rate from 0.1 to 0.3 at lower strain rates (1.25×10^{-4} to 1 s^{-1}). At higher strain rates (1000–1700 s^{-1}), the instantaneous strain hardening exponent of tin was as high as 0.5 at small strains and decreased to 0.05 at larger strains.

Fig. 9 shows the instantaneous strength coefficient of the investigated materials as a function of plastic strain. The instantaneous strength coefficient of titanium generally increases with strain rate. At strain rates from 1.25×10^{-4} to 1 s^{-1}, the strength coefficient increased from roughly 700 MPa at lower strains up to 1400 MPa at higher plastic strains. The instantaneous strength coefficient at the strain rate of 1 s^{-1} becomes lower than that observed at strain rates of 1.25×10^{-4} and 10^{-2} s^{-1} due to the thermal softening caused by adiabatic heating. At higher strain rates, from 600 up to 2300 s^{-1}, the strength coefficient increased from 800 MPa at lower plastic strains to 1800 MPa at higher plastic strains. The strength coefficient of iron at lower strain rates (1.25×10^{-4} to 1 s^{-1}) increased from roughly 500 MPa at early stages of deformation up to 600 MPa at plastic strain of approximately 0.30. As strain softening was observed in iron at higher strain rates (500 to 2400 s^{-1}), the strength coefficient is not appropriate to investigate the mechanical behavior of the material in that strain rate range. The strength coefficient of copper increased with strain rate and was somewhat constant as a function of strain. It was of approximately 350 MPa at strain rates from 1.25×10^{-4} to 1 s^{-1} and of roughly 450 MPa at strain rates from 1300 to 3100 s^{-1}. The instantaneous strength coefficient of tin at strain rates of 1.25×10^{-4} and 10^{-2} s^{-1} was constant and of 20 and 30 MPa, respectively. At the strain rate of 1 s^{-1}, the strength coefficient increased from 40 MPa in the beginning of plastic deformation to 90 MPa at plastic strain of 0.11 and decreased to 70 MPa at plastic strain of approximately 0.30. The instantaneous strength coefficient was similar at higher strain rates (1000 to 1700 s^{-1}), it increased from a lower value up to a maximum 600 MPa at a plastic strain of 0.05, decreased to 200 MPa at a plastic strain of 200 MPa, and remained roughly constant throughout the remainder of the deformation.

Fig. 10 shows the integral Taylor–Quinney coefficient, β_{int}, as a function of plastic strain. By definition, β_{int} describes the general development of β and tends to be more stable and less noisy, as it considers the total plastic work and ΔT that occurred until a given moment of the test. The β_{int} of titanium increased from 0.5 in the beginning of the experiment to 0.9 at a plastic strain of 0.15 at strain rates from 1200 to 2300 s^{-1}. At low strains, a lower β_{int} of 0.3 was observed at strain rate of 600 s^{-1}, which increased to 0.55 at a plastic strain of 0.06 and a strain rate 600 s^{-1}. The β_{int} of iron was approximately 0.5 for all investigated strain rates at low strain ($\varepsilon<0.05$). At the strain rates of 1200 and 2400 s^{-1}, β_{int} increased with strain to 0.8, decreased and stabilized at approximately 0.9 towards larger plastic strains. The β_{int} of copper at

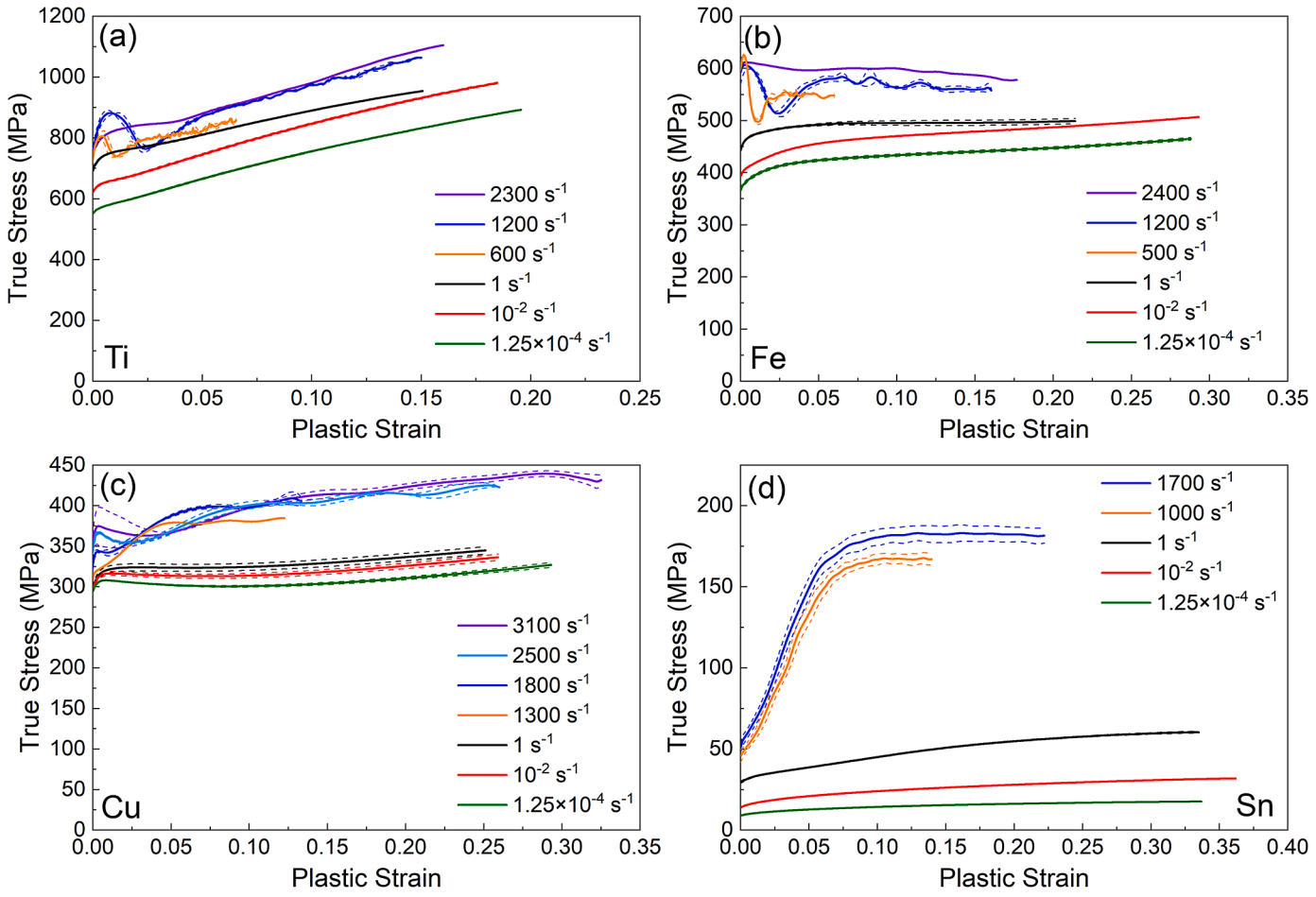

Fig 6. Compression true stress as a function of true plastic strain for Ti (a), Fe (b), Cu (c) and Sn (d) at strain rates ranging from 1.25×10^{-4} to 3100 s^{-1}.

strain rates from 1300 to 3100 s^{-1} decreased down to roughly 0.7 in the early stages of deformation ($\varepsilon<0.05$), and then gradually increased to 0.85 at plastic strains of 0.2. At both 1000 s^{-1} and 1700 s^{-1}, the β_{int} of tin was of approximately 0.25 at low strain values ($\varepsilon<0.075$) and rapidly increased to 0.85 at larger plastic strains at the strain rate of 1700 s^{-1}. The β_{int} of all investigated materials increased from a starting value up to values of approximately 0.8–0.9 and then stabilized at this higher value if given enough plastic strain.

Fig. 11 shows the differential Taylor–Quinney coefficient, β_{diff}, as a function of plastic strain. Considering that the β_{diff} is calculated using the time derivatives of plastic work and ΔT, it can better describe how the β and the microstructure evolve at any given moment during the test. Unfortunately, the differentiation makes the β_{diff} also a lot noisier than β_{int}, so a smoothing process was applied to the β_{diff}. The datasets had from 150 to 300 points, the smoothing method was adjacent-averaging with a points of window from 50 to 100, using a weighted average and no boundary conditions. In general, the β_{diff} was similar to β_{int} up to intermediate strains (ε=0.10–0.15) but it reached higher peak values from 0.95 up to 1.2. The β_{diff} then generally decreased after reaching their maximum value at intermediate values, forming what could be described as gaussian curves. The β_{diff} for titanium and iron increased with plastic strain from roughly 0.5 up to 1–1.2 before decreasing. At the strain rate of 1700 s^{-1}, the β_{diff} of tin increased to 1.2 at a plastic strain of 0.15 plastic strain and then decreased to approximately 1.1 and remained constant. The β_{int} and β_{diff} of copper were similar, as β_{diff} increased gradually with plastic strain from 0.75 to 0.95 (peak at 0.17 strain) and then decreased and remained constant at β_{diff} of 0.85 at higher strains. Although a decrease in β_{diff} was not observed at the lowest strain rates for each material, it could be associated to the low total plastic strain in those tests.

4. Discussion

The strain hardening of titanium was similar for strain rates from 1.25×10^{-4} to 10^{-2} s^{-1} and 1200 to 2300 s^{-1}, and it was characterized by strain hardening rates from 1000 to 2500 MPa, an instantaneous strain hardening exponent that increased from 0 to 0.25, and a strength coefficient that increased from 800 MPa to 1800 MPa. A positive strain rate sensitivity was observed at strain rates from 1.25×10^{-4} up to 600 s^{-1}, as there was an increase in yield strength of approximately 100 MPa for each 10^2 s^{-1} increment in strain rate. However, the increase in yield strength and strain hardening were minimal at strain rates of 1200 to 2300 s^{-1} and the mechanical behavior was quite comparable. Adiabatic heating at strain rates of 1 and 600 s^{-1} (~1.5 °C/%) lowered the strain hardening rate from 2250 MPa to 1500 MPa and the instantaneous strain hardening exponent from 0.25 to 0.175. The instantaneous strength coefficient at those strain rates was also slightly lower than that of a strain rate of 10^{-2} s^{-1}. Although adiabatic heating is even higher at the highest strain rates of 1200 and 2300 s^{-1}, strain rate hardening seemingly compensated for the thermal softening as the strain hardening behavior is similar to that observed at low strain rate (1.25×10^{-4} to 10^{-2} s^{-1}). The observed higher strain hardening at the strain rates of 1200 and 2300 s^{-1} could be related to enhanced twinning occurring at high strain rates [10,11,40]. Higher β_{int} (0.5 to 0.95) and β_{diff} (0.5 to 1.2) were observed at the highest strain rates (1200–2300 s^{-1}). This suggests that the adiabatic heating of titanium is strain and strain rate dependent, and that it converts plastic work into heat more efficiently at higher strain rates (1200 and 2300 s^{-1}) than at intermediate strain rates (600

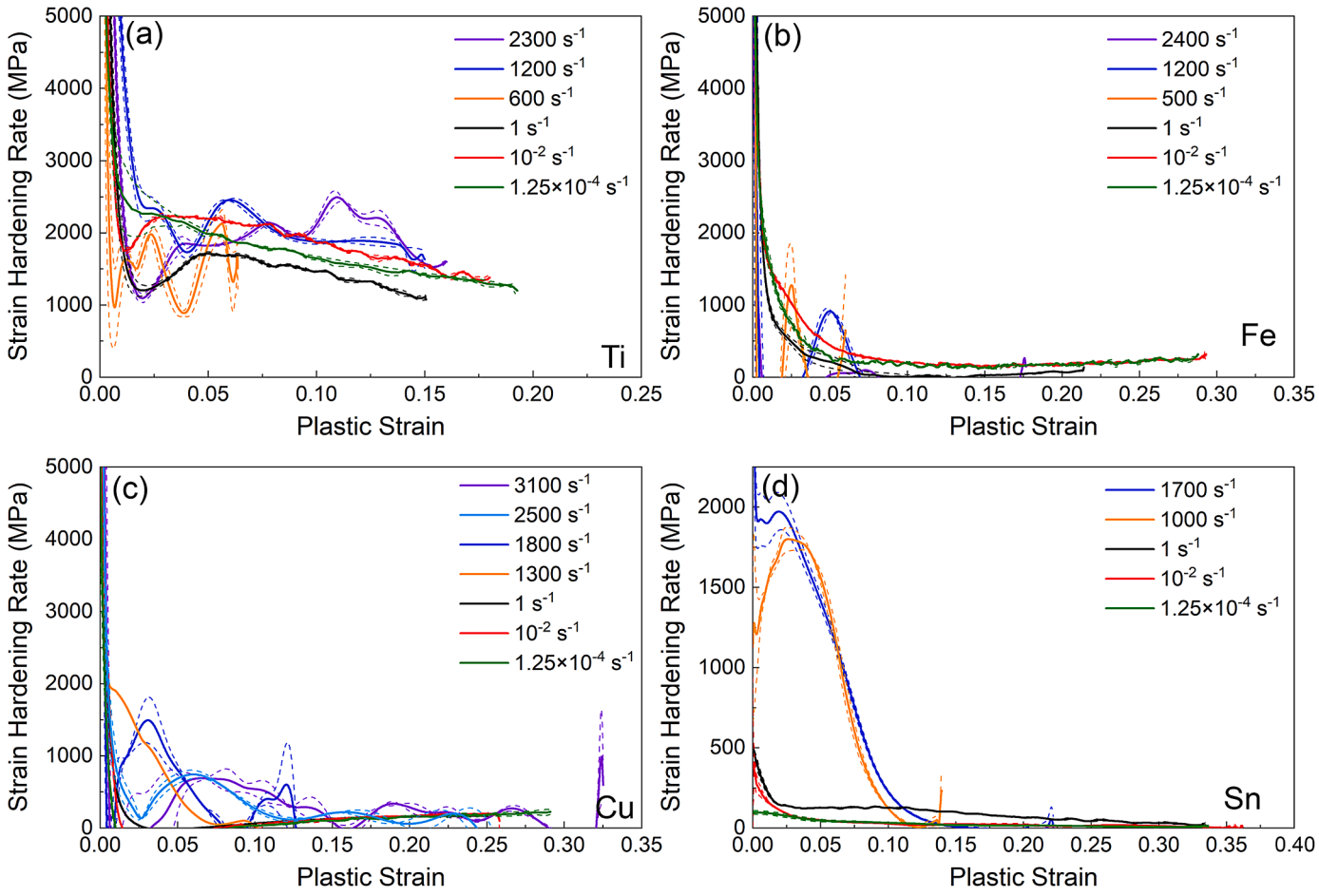

Fig 7. Strain hardening rate as a function of true plastic strain for Ti (a), Fe (b), Cu (c) and Sn (d) at strain rates ranging from 1.25×10^{-4} to 3100 s^{-1}.

s^{-1}). Similar results for an α-titanium have already been published in the literature, as Kapoor and Nemat–Nasser [41] reported a β of at least 0.6 for a strain rate of 3000 s^{-1}, Hodowany et al. [42] reported a β_{int} of approximately 0.8 for 3000 s^{-1}, and Rittel et al. [31] measured an average β_{int} that ranged from 0.9 to 0.7 in compression tests at strain rates of 2000–3000 s^{-1}. These investigations [31,41,42] were carried out using infrared detectors, and it is reassuring that the results in this current work are similar, even though the current work was carried out with different equipment. Despite the literature values of β_{int} being somewhat similar to those found in this investigation at intermediate plastic strains (ε>0.15), the β_{int} reported by Hodowany et al. [42] and Rittel et al. [31] are already as high at lower strains and either slightly decreases or does not change considerably. This difference in the results could be related to the thermomechanical history of the materials used in the studies being different. Kositski and Mordehai [43] have shown that different initial states lead to differences in β_{int} and β_{diff} at low strain levels. Nevertheless, Hodowany et al. [42] also reported an increasing β_{int} from 0.8 up to 1 for titanium with successive compressive loading at 3000 s^{-1}, which partially matches the behavior observed in this investigation. Although there are already several reports in the literature that investigated β_{int} of titanium, there has not yet been any reports on how β_{diff} of titanium changes with strain. In their work, Rittel et al. [31] reported experimental evidence indicating that the energy stored into the microstructures of titanium was lower when mechanical twins were observed in the microstructure. They observed considerable amount of twinning when the material was deformed dynamically in compression and shear for which the β_{int} were high (0.7–0.95), but almost no twinning was observed in dynamic tension for which the β_{int} was considerably lower (0.45–0.65). This is in agreement with the work from Padilla et al. [28], who concluded that most of the plastic work used for mechanical twinning is converted into heat.

The strain hardening of iron was modest at the lowest strain rates (1.25×10^{-4} and 10^{-2} s^{-1}), it diminished at a strain rate of 1 s^{-1} due to adiabatic heating, and turned into strain softening at the high strain rates (500–2400 s^{-1}). Although the strain hardening rate and instantaneous strain hardening exponent were the highest at the lowest strain rates, they were still solely of 200 MPa and 0.15, respectively. These parameters were even lower at a strain rate of 1 s^{-1} and were mostly negative for the high strain rates. A similar strain softening in iron has also been reported in other studies and has explained by unstable deformation and shear localizations [44] or with thermal softening exceeding strain hardening [9]. At low strains (ε<0.05), β_{int} and β_{diff} were of approximately 0.5 at the strain rates of 500 to 2400 s^{-1}. At the strain rate of 2400 s^{-1}, β_{int} increased up to 0.9 at a plastic strain of 0.15 and was relatively constant thereafter. β_{diff} increased up to 1.1 and 1.2 at the strain rates of 1200 and 2400 s^{-1}, respectively. For iron, the β_{int} and β_{diff} increased faster at higher strain rates. Rittel et al. [31] reported similar β_{int} values of 0.85 for a 1020 carbon steel under compression at strain rates of 1400 s^{-1}, which is similar to the β_{int} value observed for iron in plastic strains higher than ε=0.15 in this investigation. However, the β_{int} reported by Rittel et al. does not increase at lower plastic strain values as it is already 0.95 at plastic strains of 0.05. Although initially lower, the β_{int} in this investigation grows to a similar value to the β value of 0.865 reported by Farren and Taylor [26] for an annealed steel and the 0.9–0.97 range reported by Taylor and Quinney [27] for a decarburized mild steel. Similar to what was mentioned for titanium, these differences between the β found in the in the literature and those reported in this worked could be partly explained by the investigated

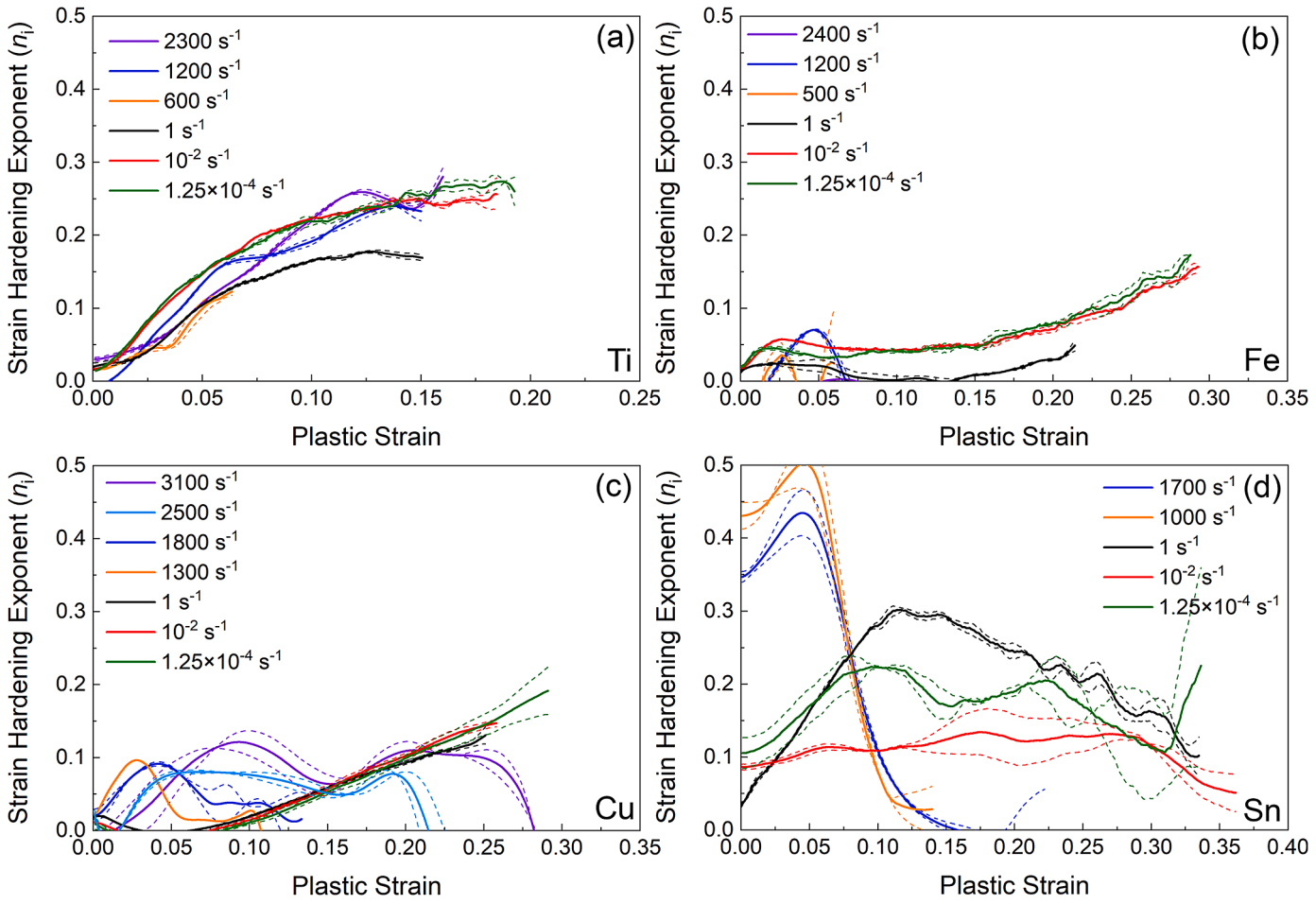

Fig 8. Instantaneous strain hardening exponent as a function of true plastic strain for Ti (a), Fe (b), Cu (c) and Sn (d) tested under compression from strain rates from 1.25×10^{-4} to 3100 s^{-1}.

materials having a different cold work history and, thus, a different initial state.

The mechanical behavior of copper was characterized by yield strength from 300 to 370 MPa, low strain hardening rate (<1500 MPa), low instantaneous strain hardening exponent (up to 0.15) and an almost constant instantaneous strength coefficient of approximately 400 MPa. Almost no strain hardening occurred at low strain rates (1.25×10^{-4} to 1 s^{-1}) and a similar modest strain hardening behavior was observed at the higher strain rates (1300 to 3100 s^{-1}). β_{int} and β_{diff} of copper were not strain rate dependent. At strain rates from 1300 to 3100 s^{-1}, β_{int} increased from approximately 0.7 up to a saturation value of 0.8 while, while β_{diff} increased from 0.7 to 0.95 at intermediate strains (ε=0.15) and decreased to 0.8 at larger strains. Although β_{int} is marginally lower, the results of this investigation are in agreement with those presented by Farren and Taylor [26] and Taylor and Quinney [27]. These authors reported β values ranging from 0.905 to 0.92 [26] and from 0.89 to 0.96 [27] in pure copper and proposed that β is constant throughout plastic deformation. This is in accordance with the results from this study, in which a mostly constant β_{int} and β_{diff} were observed throughout plastic deformation and β_{diff} was similar to those presented in those papers. However, Rittel et al. [5] has also investigated average β_{int} in polycrystalline copper and reported a value of approximately 0.5 for at a strain rates of roughly 3000 s^{-1}, which was considerably lower than that found in this work. Nevertheless, the authors also reported an average β_{int} of 0.75 for a strain rate of 1.7 s^{-1}, which very similar to that found at higher strain rates in this investigation.

The strain hardening of tin was characterized by a single stage at low strain rates (1.25×10^{-4}–1 s^{-1}) with low true stresses (10–50 MPa), low strain hardening rate (0–500 MPa), a low to medium instantaneous strain hardening exponent (0.1–0.3), and a low instantaneous strength coefficient (20–90 MPa). At higher strain rates (1000–1700 s^{-1}), two distinct strain hardening stages were observed. A large and rapid increase in true stress (50–180 MPa) with a comparatively high strain hardening rate (1500–2000 MPa), a high instantaneous strain hardening exponent (0.3–0.5), and a high strength coefficient (550–600 MPa) were observed in the first strain hardening stage (ε<0.1). The strain hardening rate (0–250 MPa), the instantaneous strain hardening exponent (0–0.1), and the strength coefficient (200 MPa) of the second stage were low. Considering that a very low strain hardening rate and an approximately constant instantaneous strain hardening exponent and strength coefficient were observed for tin at the lowest strain rates (1.25×10^{-4}–10^{-2} s^{-1}) and a peak with very high strain hardening rate, instantaneous strain hardening exponent and strength coefficient, it is possible that an intermediate behavior between both strain rate ranges is occurring at 1 s^{-1}, as instantaneous strain hardening exponent and strength coefficient clearly shows a similar peak and a higher strain hardening rate throughout that whole test. The low β_{int} and β_{diff} values (0.2) of the first strain hardening stage (ε<0.05) indicate that most of the imposed plastic work (~80%) is being stored in the microstructure. It is noteworthy that the differential nature of β_{diff} makes it more suitable for investigating the instantaneous strain hardening behavior of a material, as the increase in β_{diff} occurs simultaneously with the beginning of the second strain hardening stage, while β_{int} starts increasing at slightly higher strains due to its integral nature. The second strain hardening stage at the strain rates of 1000 and 1700 s^{-1} had an increasing β_{int} (from 0.2 to 0.85) and β_{diff} (0.2 to 1.2). This suggests that different

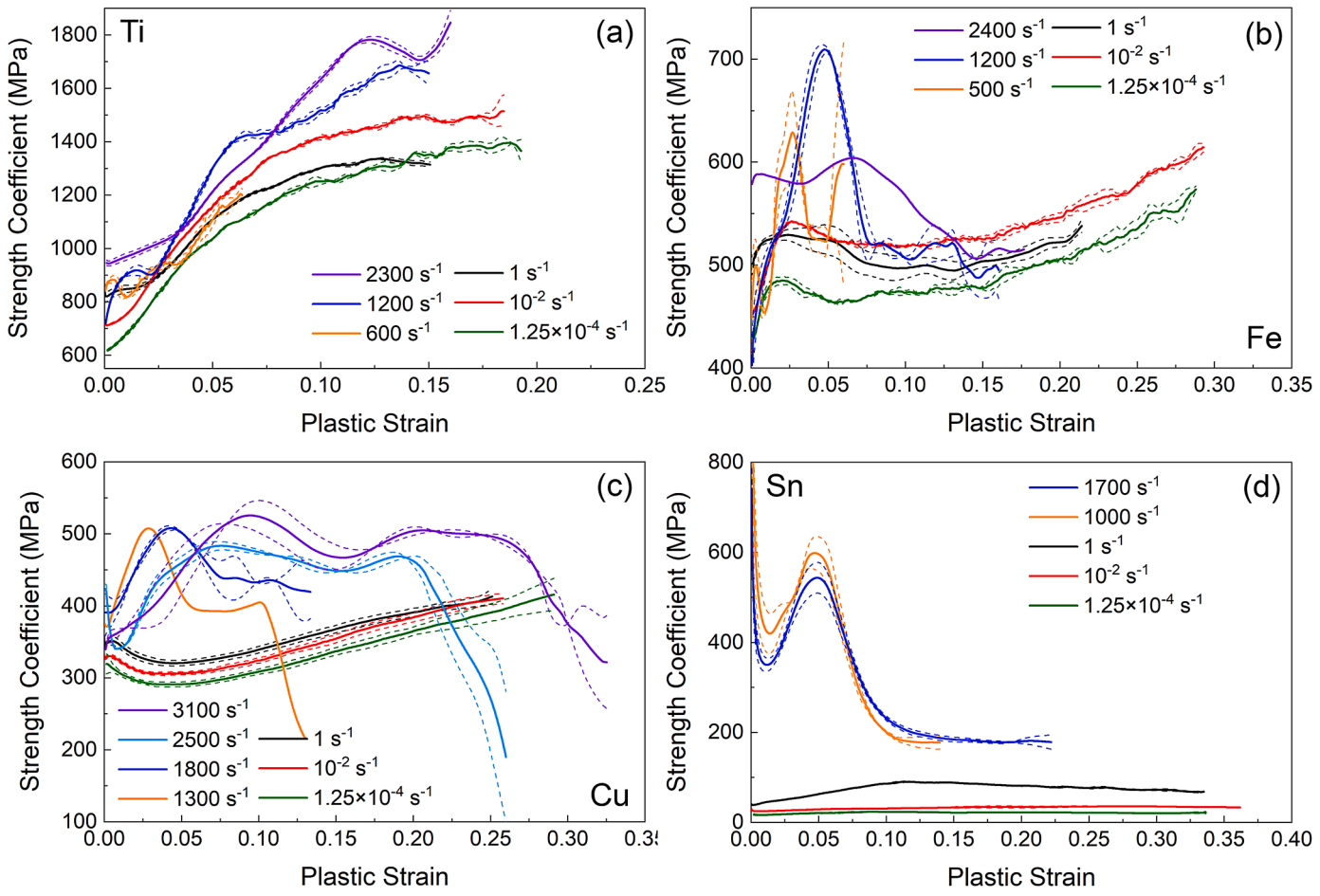

Fig 9. Instantaneous strength coefficient as a function of true plastic strain for Ti (a), Fe (b), Cu (c) and Sn (d) tested in compression at strain rates from 1.25×10^{-4} to 3100 s^{-1}.

deformation mechanisms are active in the first and second strain hardening stages. A dashed line separates both strain hardening stages in Fig. 7(d) to assist the visualization of these distinct β_{diff} values. A two stage strain hardening behavior at high strain rates characterized by a first strain hardening stage with higher strain hardening rate at lower strain values and a second strain hardening stage with much lower strain hardening strain rate have also been reported in other investigations for tin alloys [1,4,45–47]. An analogous two-staged strain hardening behavior has also been observed in tensile loading at intermediate and high strain rates [47,48]. Considering that most plastic work is converted into heat during mechanical twinning [28], it is possible that the increase in β with strain is related to an increase in twinning activity after a plastic strain of approximately 0.05 at high strain rates. Perez-Bergquist et al. [45] associated the occurrence of grain coarsening to a decrease in strain hardening rate at higher strains in tin alloys. Alden [49] investigated the deformation mechanisms Sn-5%Bi alloy and concluded that grain boundary sliding is the main mechanisms at low strain rates while dislocation slip is dominant at high strain rates. Boyce et al. [50] associated grain boundary sliding as the dominant deformation mechanisms on a eutectic Sn-Pb alloy, and reported that at high strain rates grains were broken into smaller subgrains with similar orientation, while grains with high angle boundaries and distinct orientation were observed after deformation at lower strain rates. While it is possible that a combination of grain coarsening, dislocation slip and grain boundary sliding is responsible for the behavior observed in tin at high strain rates, further investigation is necessary to pinpoint what were the mechanisms responsible for the increase in β_{int} and β_{diff} in the second strain hardening stage. Régal and Pierron [30] used Image-Based Ultrasonic Shaking and reported a β for tin that decreased from 0.9 at lower strains to 0.6 at larger strains, which indicates a different trend from that found in this investigation. Nevertheless, their investigation was based on cyclic deformation, which develops higher dislocation densities and vacancy concentrations with corresponding cumulative plastic strains, which imply a higher amount of energy stored in the microstructure and could explain the lower β.

Considering that β in general is a measure of how much plastic work is converted into heat during plastic deformation, it is logical to conclude that the leftover energy is used for microstructural evolution. Following this line of thought, a β_{int} of one indicates a material with a perfectly stable microstructure that converts all plastic work into heat and a β_{int} of 0 would indicate a material with a fast evolving microstructure that stores all plastic work into defects into the microstructure. The β_{int} of all investigated materials were lower (0.2–0.7) at low strains and generally increased up to higher values (0.8–0.95) at intermediate strains. In case β_{int} already had reached a maximum by a given plastic strain, these higher β_{int} values remained constant through the rest of the experiment. This is plausibly related to plastic work initially being used to evolve the microstructure (lower β_{int} and β_{diff}), as point and line defects are generated and stored, but which ultimately leads to a saturated microstructure, which converts most of the plastic work into heat (higher β_{int} and β_{diff}). This is in accordance with the work from Kositski and Mordehai [43], who have shown with molecular dynamics simulations that β_{int} and β_{diff} increase in the first stage of deformation due to an increase in the defect volume fraction and energy stored in the grain boundaries. Their simulations also suggested that above a strain value (10% in their work) there tends to be an equilibrium between generation

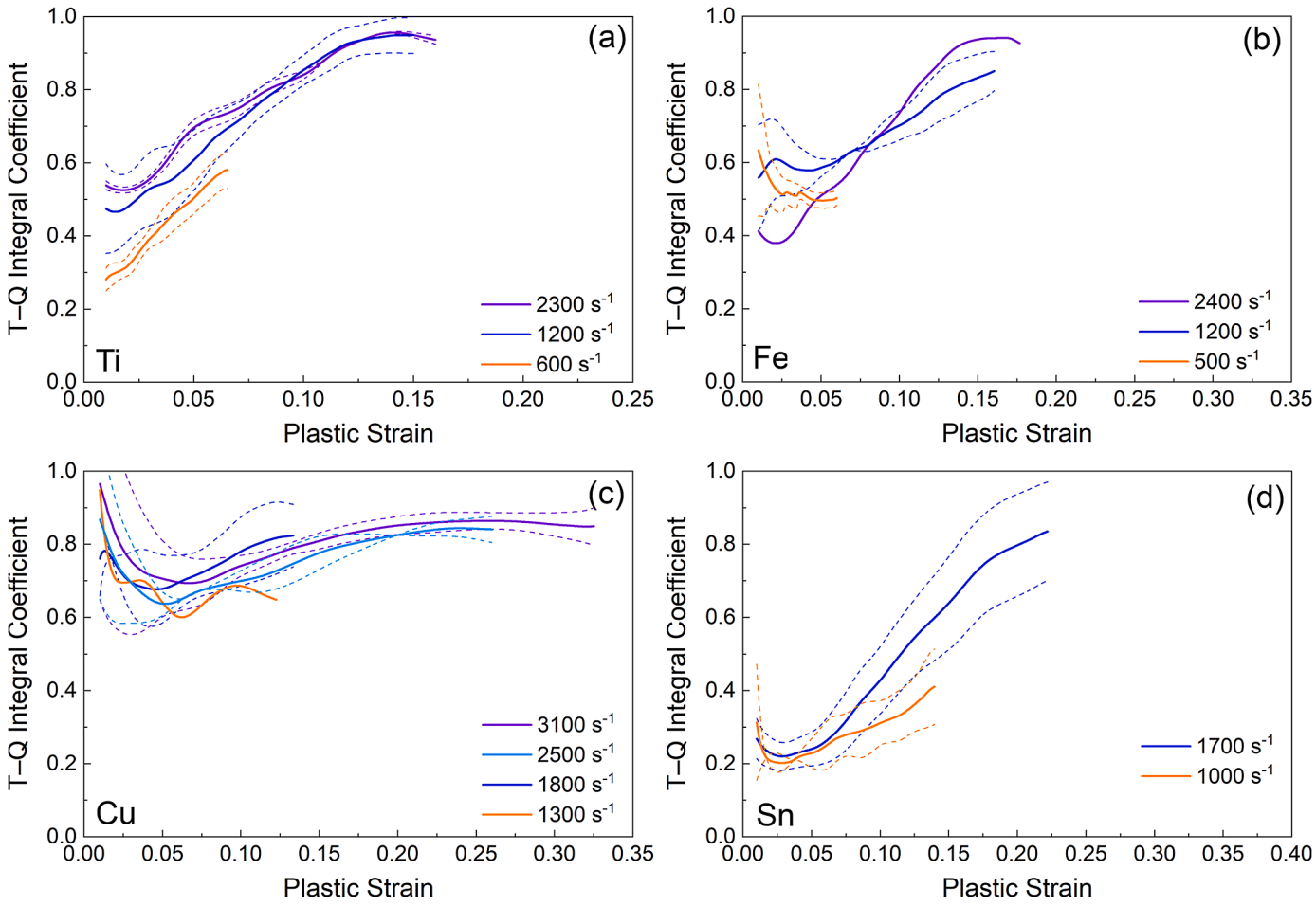

Fig 10. Integral Taylor–Quinney coefficient as a function of true plastic strain for Ti (a), Fe (b), Cu (c) and Sn (d) at strain rates ranging from 1.25×10^{-4} to 3100 s^{-1}.

and annihilation of dislocations, leading to a β_{diff} close to one. According to the results from this work, this plastic strain at which this saturation occurs apparently decreases with increasing strain rate, and it is known that the saturation strain will be different according to the initial state of the microstructure [43]. This strain rate dependence could be a result of higher strain rates causing reduced dislocation cross-slip and a more uniform dislocation substructure for an equivalent amount of plastic strain [12]. It is possible that the structure of a material deformed at higher strain rates could reach a uniform and saturated condition faster due to reduced cross-slip and dynamic recovery. Similar results in which β_{int} increased from a lower value to nearly 1 and remaining constant with further increasing strain have also been reported by Hodowany et al. [42] for titanium and a 2024-T4 aluminum alloy that were loaded in several sequences. The specimens were loaded several times to reach large plastic deformations (up to 0.6) and the beta increased to close to 1 at large plastic strains. Rittel et al. [8] also reported that the β_{int} in iron in dominant shear at a strain rate of 8400 s^{-1} increased from a lower value (0.6) up to values as high as 1.15 at higher strains (ε =0.5). and moderately decreasing to 1.05 at plastic strains of 0.7. The occurrence of dynamic recrystallization and its exothermal nature were associated with the observed $\beta_{int}>1$. In their studies on the thermomechanical behavior of single crystalline tantalum, Rittel et al. [51] observed a similar increase in β_{int} to nearly 1 in single crystals with [110] orientation, but observed a much lower β_{int} in [100] orientated single crystals. Rittel et al. [51] suggested that the grains with the [110] orientation have a stronger role in the plastic deformation of polycrystalline tantalum than the [100] oriented grains, as the β_{int} of the single crystals with [110] orientation was much more similar to that of the polycrystalline tantalum [52].

Analogously to its integral counterpart, β_{diff} increased from lower values (0.2–0.7) up to a maximum (0.95–1.2) at intermediate strains and then decreased towards larger plastic strains. According to Rittel [16], the development of such gaussian curves in β_{diff} always occurs in the thermal softening domain of the deformation and could be associated with the release of stored energy from the microstructure. The plastic strain associated with this maximum in β_{diff} was the same as that β_{int} saturated. The evolution of the microstructure is a continuous process in which energy is simultaneously stored and released as dislocations and other defects are formed and annihilated. The β_{diff} higher than 1 can occur when there is high momentary release of energy at a given moment due to the dynamic recovery of dislocations [16]. Although in an experiment with cyclic deformation, Dillon [53] has also reported that the rate of heat generation can be higher than the rate in which plastic work is applied in adiabatic conditions. The mechanisms which could lead to β_{diff} exceeding one are not yet fully understood, although there seem to be indications in the literature that it can occur and that it could be related to dynamic recovery and the release of energy stored in the microstructure. Kositski and Mordehai [43] have shown with molecular dynamics simulations that β_{diff} can be bigger than 1 if plastic strain leads to rearrangement of grain boundaries. To fully address this matter, extensive SEM and TEM investigations on the evolution of the microstructure and dislocation substructure, as well as simulations on the molecular level are needed to understand the underlying mechanisms in which microstructural energy is released during plastic deformation.

Based on the previous interpretation of β_{int} and β_{diff}, copper seems to have the most stable microstructure and tin would have the microstructure that evolved the most during plastic deformation. The β_{int} and

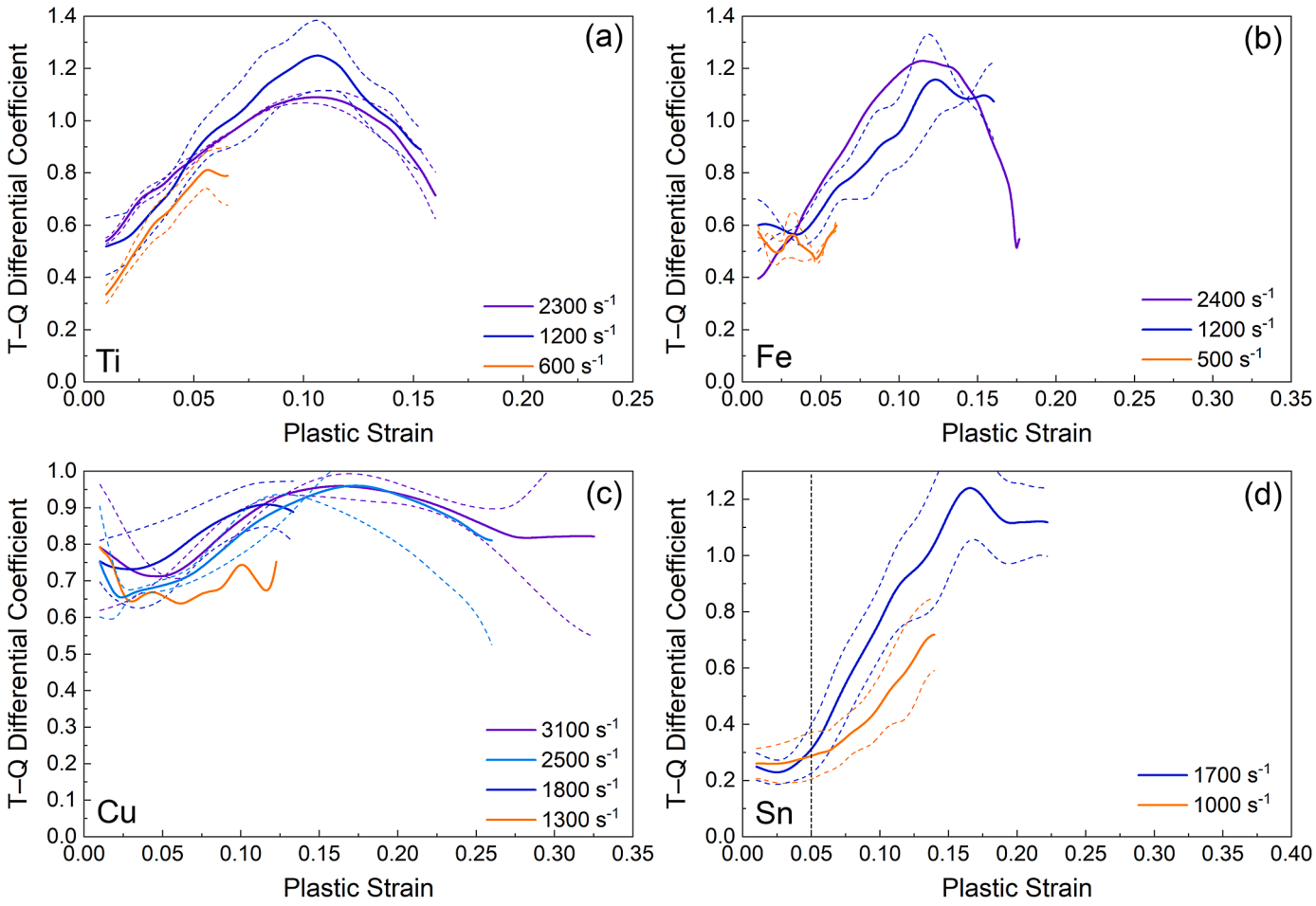

Fig 11. Differential Taylor–Quinney coefficient as a function of true plastic strain for Ti (a), Fe (b), Cu (c) and Sn (d) at strain rates ranging from 1.25×10^{-4} to 3100 s^{-1}. The dashed line on (d) separate the first and the second strain hardening stage which have different β_{diff} values.

β_{diff} of titanium and iron were similar and somewhat intermediate to that observed in copper and tin. Strain hardening rate and the instantaneous strain hardening exponent also describe the rate at which the microstructure evolves. The instantaneous strength coefficient provided further information on how the mechanical resistance of the materials evolved. Analyzing the strain hardening parameters lead to similar conclusions on the evolution of the microstructure as the interpretation of the Taylor–Quinney coefficients. The strain hardening rate and the instantaneous strain hardening exponent of copper were low, with an almost constant strength coefficient, which also suggest a stable microstructure that does not change much during deformation. The first strain hardening stage of tin was characterized by a high instantaneous strain hardening exponent (~0.5), a comparably high strain hardening rate (~2000 MPa), and a high strength coefficient (600 MPa) which implies a faster evolving microstructure. At larger plastic strains, little to no increase in true stress, a low strain hardening rate, a low instantaneous strain hardening exponent and strength coefficient were observed for tin, which would be characteristic of a stable microstructure. Despite the β_{int} and β_{diff} of both titanium and iron having similar values, they had reasonably different strain hardening behavior. Titanium had a positive strain hardening rate, an intermediate instantaneous strain hardening exponent (up to 0.25) and an increasing strength coefficient, corroborating the storage of energy in its microstructure during plastic deformation. Nevertheless, strain softening was observed for iron during plastic deformation, which does not readily fit the hypothesis of a moderately evolving microstructure that stored energy during plastic deformation. Although the relationship between β, strain hardening parameters and microstructural evolution being in agreement with what was observed for titanium, copper, and tin, this relationship still requires further investigation to be better understood and applied to material research.

5. Summary and conclusions

The effects of adiabatic heating and strain rate on the dynamic compressive behavior of commercially pure tin, copper, iron, and titanium were investigated at quasi-static (1.25×10^{-4}–1 s^{-1}) and dynamic (600–3100 s^{-1}) strain rates. The experiments were monitored by a high speed infrared camera to record the temperature evolution of the specimens during the experiment. The radiometric temperature measurements from the infrared camera were converted to true surface temperatures using K-type thermocouples. By combining the load, strain, and temperature data for different strain rates, it was possible to evaluate the effects of adiabatic heating on the thermomechanical behavior of these metals by analyzing the temperature increase and calculating the Taylor–Quinney coefficients at different strain rates. The mechanical behavior and the microstructural evolution of the materials were discussed and analyzed in terms of strain hardening parameters, ΔT, β_{int}, and β_{diff}. The following conclusions can be drawn from this investigation:

(I) A positive strain rate sensitivity was observed for all the investigated materials. However, a notable decrease in strain hardening rate with increase in adiabatic heating was observed for iron and titanium when the strain rate was increased from 1.25×10^{-4} to 1 s^{-1}. The increase in temperature of copper and tin

was low and did not seem to have a noticeable impact on the strain hardening of these metals at the studied range of plastic strain.

(II) Adiabatic heating of all materials increased with strain rate. At the lowest strain rates (1.25×10^{-4} and 10^{-2} s^{-1}) the heating was very low with a maximum ΔT of roughly 2.5 °C, while a maximum of temperature increase of 65 °C was observed for titanium at the strain rate of 2300 s^{-1}.

(III) β_{diff} seems to be a more appropriate parameter for describing the thermomechanical behavior of materials, while β_{int} is more useful for applications which require a single digit parameter to describe how efficiently a material transforms plastic work into heat up to a certain strain level. The reason being that β_{int} calculation considers the entire plastic work and temperature increase until a given moment and β_{diff} is based on the time differentials of these quantities.

(IV) The β_{int} of all investigated materials increased from a lower value (0.2–0.7) with strain and generally stabilized at a saturation value of roughly 0.8–0.95. The shape of the β_{diff} plots could be described as gaussian curves which has maximum values up to 1.2 at intermediate strains and then decreased at the strain in which β_{int} reached its saturation value. These higher than 1 β_{diff} values imply that the rate of heat generation at those moments was higher than the rate at which plastic work was been applied, plausibly as a result of the release of energy stored in the microstructure during dynamic recovery.

(V) β_{int}, β_{diff} and the strain hardening parameters led to similar conclusions when qualitatively evaluating how stable the microstructures of titanium, copper, and tin were during plastic deformation. Copper had a high β_{int}, a low instantaneous strain hardening exponent, and strain hardening rate, and a constant instantaneous strength coefficient, evidencing the stability of its microstructure throughout plastic deformation. Tin had a first strain hardening stage with a low β_{int} and β_{diff}, a high instantaneous strain hardening exponent and strain hardening rate, and a maximum in its strength coefficient, which suggested a faster evolving microstructure. The second strain hardening stage of tin was characterized by an increasing β_{int} and β_{diff} associated with a low instantaneous strain hardening exponent and strain hardening rate, and its strength coefficient reached a minimum and plateaued, characteristic of a more stable microstructure. In comparison to copper and tin, titanium had intermediate β_{int} and β_{diff} values, strain hardening rate and instantaneous strain hardening exponent values, and a strength coefficient that steadily increased with plastic strain, indicating a material which stored energy during its plastic deformation but just not as efficiently as tin at low strain values.

CRediT authorship contribution statement

G.C. Soares: Methodology, Investigation, Software, Formal analysis, Data curation, Writing – original draft, Writing – review & editing, Visualization. **M. Hokka:** Project administration, Funding acquisition, Resources, Supervision, Writing – review & editing.

Declaration of Competing Interest

The authors declare that they have no known competing financial interests or personal relationships that could have appeared to influence the work reported in this paper.

Acknowledgements

This research received funding from Tampere University. This research did not receive any specific grant from funding agencies in the public, commercial, or not-for-profit sectors.

References

[1] Chen X, Zhou J, Xue F, Yao Y. Mechanical deformation behavior and mechanism of Sn-58Bi solder alloys under different temperatures and strain rates. Mater Sci Eng A 2016;662:251–7.
[2] Zhang S, Wang YC, Zhilyaev AP, Gunderov DV, Li S, Raab GI, et al. Effect of temperature on microstructural stabilization and mechanical properties in the dynamic testing of nanocrystalline pure Ti. Mater Sci En, A 2015;634:64–70.
[3] Zaretsky EB, Kanel GI. Dynamic response of Sn over the temperature range 115–503 K. In: DYMAT 2009 - 9th International Conferences on the Mechanical and Physical Behaviour of Materials under Dynamic Loading, Les Ulis, France; 2009.
[4] Siviour CR, Walley SM, Proud WG, Field JE. Mechanical properties of SnPb and lead-free solders at high rates of strain. J Phys D Appl Phys 2005;38(22):4131–9.
[5] Rittel D, Kidane AA, Alkhader M, Venkert A, Landau P, Venkert A, et al. On the dynamically stored energy of cold work in pure single crystal and polycrystalline copper. Acta Mater 2012;60(9):3719–28.
[6] Apostol M, Kuokkala V-T, Vuoristo T. High temperature high strain rate behavior of OFHC copper with a compressive high temperature recovery split hopkinson pressure bar. In: Proceedings of ICEM12 - 12th International Conference on Experimental Mechanics, Bari; 2004.
[7] Muller T. High strain rate behaviour of iron and nickel. J Mech Eng Sci 1972;14(3):161–7.
[8] Rittel D, Ravichandran G, Venkert A. The mechanical response of pure iron at high strain rates under dominant shear. Mater Sci Eng, A 2006;432(1–2):191–201.
[9] Bao WP, Xiong ZP, Ren XP, Wang FM. Effect of strain rate on mechanical properties of pure iron. Adv Mat Res 2013;705:21–5.
[10] Gurao NP, Kapoor R, Suwas S. Deformation behaviour of commercially pure titanium at extreme strain rates. Acta Mater 2011;59(9):3431–46.
[11] Gray GT. Influence of strain rate and temperature on the structure. Property behavior of high-purity titanium. Le J Phys IV 1997;07.
[12] Gray III GT. High-Strain-Rate Deformation: mechanical Behavior and Deformation Substructures Induced. Annu Rev Mater Res 2012;42(1):285–303.
[13] Yang F, Li JC. Deformation behavior of tin and some tin alloys. J Mater Sci: Mater Electron 2007;18(1–3):191–210.
[14] Rittel D. Transient temperature measurement using embedded thermocouples. Exp Mech 1998;38(2):73–8.
[15] Rittel D. Experimental investigation of transient thermoelastic effects in dynamic fracture. Int J Solids Struct 1998;35(22):2959–73.
[16] Rittel D. On the conversion of plastic work to heat during high strain rate deformation of glassy polymers. Mech Mater 1999;31(2):131–9.
[17] Zhou M, Rosakis AJ, Ravichandran G. Dynamically propagating shear bands in impact-loaded prenotched plates - II. Numerical simulations. J Mech Phys Solids 1996;44(6):1007–21.
[18] Zehnder A, Rosakis A. On the temperature distribution at the vicinity of dynamically propagating cracks in 4340 steel. J Mech Phys Solids 1991;39(3):385–415.
[19] Marchand A, Duffy J. An experimental study of the formation process of adiabatic shear bands in a structural steel. J Mech Phys Solids 1988;36(3):251–83.
[20] Zhang LH, Rittel D, Osovski S. Thermo-mechanical characterization and dynamic failure of near α and near β titanium alloys. Mater Sci Eng, A 2018;729:94–101.
[21] Smith JL, Seidt JD, Gilat A. Full-field determination of the taylor-quinney coefficient in tension tests of Ti-6Al-4V at strain rates up to 7000-1. In: Advancement of Optical Methods & Digital Image Correlation in Experimental Mechanics, Volume 3. Conference Proceedings of the Society for Experimental Mechanics Series, vol. 3, Cham, Springer; 2019. p. 133–9.
[22] Gilat A, Kuokkala V-T, Seidt JD, Smith JL. Full-field measurement of strain and temperature in quasi-static and dynamic tensile tests on stainless steel 316L. Procedia Eng 2017;207:1994–9.
[23] Seidt JD, Kuokkala V-T, Smith JL, Gilat A. Synchronous full-field strain and temperature measurement in tensile tests at low, intermediate and high strain rates. Exp Mech 2017;57:219–29.
[24] Johnston JP, Pereira JM, Ruggeri CR, Roberts GD. High-speed infrared thermal imaging during ballistic impact of triaxially braided composites. J Compos Mater 2018;52(25):3549–62.
[25] Nie Y, Claus B, Gao J, Zhai X, Kedir N, Chu J, et al. In situ observation of adiabatic shear band formation in aluminum alloys. Exp Mech 2020;60(2):153–63.
[26] Farren WS, Taylor GI. The heat developed during plastic extension of metals. Proc R Soc A 1925;107(743):422–51.
[27] Taylor GI, Quinney H. The latent energy remaining in a metal after cold working. Proc R Soc A 1934;143(849):307–26.
[28] Padilla H, Smith C, Lambros J, Beaudoin A, Robertson I. Effects of deformation twinning on energy dissipation in high rate deformed zirconium. Metall Mater Trans A 2007;38(12):2916–27.
[29] Zhang LH, Rittel D, Osovski S. Thermo-mechanical characterization and dynamic failure of near α and near β titanium alloys. Mater Sci Eng, A 2018;729:94–101.
[30] Régal X, Pierron F. A new technique to measure the dynamic Taylor-Quinney coefficient. In: Proceedings of the Society for Experimental Mechanics' 2019 Annual Conference, Reno; 2019.
[31] Rittel D, Zhang LH, Osovski S. The dependence of the Taylor–Quinney coefficient on the dynamic loading mode. J Mech Phys Solids 2017;107:96–114.
[32] Gorham DA, Wu XJ. An empirical method of dispersion correction in the compressive hopkinson bar test. Le J Phys IV 2007;07:223–8.
[33] Vuoristo T. Effect of strain rate on the deformation behavior of dual phase steels and particle reinforced polymer composites (Doctoral thesis). Tampere: Tampere University of Technology; 2004.

[34] Hokka M, Kuokkala V-T, Curtze S, Vuoristo T, Apostol M. Characterization of strain rate and temperature dependent mechanical behavior of TWIP steels. J Phys IV 2006;134(EDP Sciences):1301–6.
[35] Hokka M, Leemet T, Shrot A, Baeker M, Kuokkala VT. Characterization and numerical modeling of high strain rate mechanical behavior of Ti-15-3 alloy for machining simulations. Mater Sci Eng, A 2012;550:350–7.
[36] Soares GC, Gonzalez BM, d. A. Santos L. Strain hardening behavior and microstructural evolution during plastic deformation of dual phase, non-grain oriented electrical and AISI 304 steels. Mater Sci Eng A 2017;684:577–85.
[37] Soares GC, Rodrigues MCM, d. A. Santos L. Influence of temperature on mechanical properties, fracture morphology and strain hardening behavior of a 304 stainless steel. Mater Res 2017;20(suppl 2):141–71.
[38] Soares GC, Queiroz RRU, Santos LA. Effects of dynamic strain aging on strain hardening behavior, dislocation substructure, and fracture morphology in a ferritic stainless steel. Metall Mater Trans A 2020;51(2):725–39.
[39] Davis J. Metals handbook. Desk Edition (2nd Edition). Materials Park: ASM International; 1998.
[40] Zhou P, Xiao D, Jiang C, Sang G, Zou D. Twin interactions in pure Ti under high strain rate compression. Metall Mater Trans A 2017;48(1):126–38.
[41] Kapoor R, Nemat-Nasser S. Determination of temperature rise during high strain rate deformation. Mech Mater 1998;27(1):1–12.
[42] Hodowany J, Ravichandran G, Rosakis AJ, Rosakis P. Partition of plastic work into heat and stored energy in metals. Exp Mech 2000;40(2):113–23.
[43] Kositski R, Mordehai D. Employing molecular dynamics to shed light on the microstructural origins of the Taylor-Quinney coefficient. Acta Mater 2021;205. 116511.
[44] Wei Q, Schuster BE, Mathaudhu SN, Hartwig KT, Kecskes LJ, Dowding RJ, et al. Dynamic behaviors of body-centered cubic metals with ultrafine grained and nanocrystalline microstructures. Mater Sci Eng, A 2008;493(1–2):58–64.
[45] Perez-Bergquist AG, Cao F, Perez-Bergquist SJ, Lopez MF, Trujillo CP, Cerreta EK, et al. The constitutive response of three solder materials. J Alloys Compd 2012; 524:32–7.
[46] CHUAN OK. Dynamic material characterisation of solder interconnects in microelectronic packaging. Department of Mechanical Engineering, National University of Singapore; 2005 *(Master's Thesis)*.
[47] Qin F, An T, Chen N. Strain rate effects and rate-dependent constitutive models of lead-based and lead-free solders. J Appl Mech Trans ASME 2010;77(1):1–11.
[48] Yazzie K, Williams J, Chawla N. Fracture behavior of Sn-3.5Ag-0.7Cu and pure Sn solders as a function of applied strain rate. J Electron Mater 2012;41(9):2519–26.
[49] Alden TH. The origin of superplasticity in the sn-5%bi alloy. Acta Metall 1967;15 (3):469–80.
[50] Boyce BL, Brewer LN, Neilsen MK, Perricone MJ. On the strain rate- and temperature-dependent tensile behavior of eutectic Sn-Pb solder. J Electron Packag Trans ASME 2011;133(3).
[51] Rittel D, Silva ML, Poon B, Ravichandran G. Thermomechanical behavior of single crystalline tantalum in the static and dynamic regime. Mech Mater 2009;41(12): 1323–9.
[52] Rittel D, Bhattacharyya A, Poon B, Zhao J, Ravichandran G. Thermomechanical characterization of pure polycrystalline tantalum. Mater Sci Eng, A 2007;447(1–2): 65–70.
[53] Dillon OW. The heat generated during the torsional oscillations of copper tubes. Int J Solids Struct 1966;2(2):181–204.